Nanoscale Res Lett (2010) 5:494–500
DOI 10.1007/s11671-009-9522-4

SPECIAL ISSUE ARTICLE

Finite-Element Modelling of Biotransistors

M. W. Shinwari · M. J. Deen · P. R. Selvaganapathy

Received: 25 August 2009 / Accepted: 17 December 2009 / Published online: 19 January 2010

Abstract Current research efforts in biosensor design attempt to integrate biochemical assays with semiconductor substrates and microfluidic assemblies to realize fully integrated lab-on-chip devices. The DNA biotransistor (BioFET) is an example of such a device. The process of chemical modification of the FET and attachment of linker and probe molecules is a statistical process that can result in variations in the sensed signal between different BioFET cells in an array. In order to quantify these and other variations and assess their importance in the design, complete physical simulation of the device is necessary. Here, we perform a mean-field finite-element modelling of a short channel, two-dimensional BioFET device. We compare the results of this model with one-dimensional calculation results to show important differences, illustrating the importance of the molecular structure, placement and conformation of DNA in determining the output signal.

Keywords Biosensor · Microarray · DNA · Model · Sensitivity

Introduction

Contemporary nucleic acid sequencing tools rely on optical DNA microarrays to detect successful hybridization. Due to its high cost, lack of portability, and use of labelling agents, research attention is focused on developing fully electronic, label-free DNA biosensors. Several possibilities have been investigated for such sensors, including DNA-sensitive electrodes [1–3], DNA transistors [4–7], cantilever beam DNA sensors [8, 9], optical label-free sensors [10] and nanowire and nanobead DNA sensors [11–13]. All of these methods have been shown to selectively sense complementary target DNA strands. For these devices to be commercially used, they must exhibit a high degree of repeatability and stability in their output signals. The noise contributions of the devices place an upper limit on the sensitivity of the sensor [14]. This includes electronic noise sources, noise from the reference electrodes, and noise from the random electrochemical processes. On the other hand, variations in the device due to the number, placement, and orientation of probe and linker molecules can have adverse effects on the sensed signal and can therefore cause signal variations between different cells in an array. These variations are much more significant with nanoscale sensors, where the conformation of molecules can severely distort the output signal.

To investigate the relative magnitudes of these signal variations, a model for the response of the biosensor must be formulated. In the case of the BioFET, a mean-field 1-D model for the semiconductor surface potential response was previously developed [15] and subsequently used to construct a complete 1-D model for the biotransistor [14, 16], as well as a simplified analytical model [17]. A 2-D cylindrical model of the DNA and surrounding ionic cloud was also developed [18]. In the cylindrical model, the sensitivity of the BioFET to hybridization was calculated by pinning the semiconductor's channel to a certain surface potential such that a certain current is maintained, while varying the source voltage. This approach ignores the variations of the semiconductor's charge distribution along

M. W. Shinwari (✉) · M. J. Deen
Department of Electrical Engineering, McMaster University, 1280 Main St. West, Hamilton, ON L8S 4K1, Canada
e-mail: shinwamw@mcmaster.ca

P. R. Selvaganapathy
Department of Mechanical Engineering, McMaster University, 1280 Main St. West, Hamilton, ON L8S 4L7, Canada

the device's length. Additionally, such a model would not allow the investigation of weakly inverted devices, as the channel's charge modulation is taken as a linear indicative of conductance modulation and hence, sensitivity. Here, we perform 2-D finite-element simulations on the entire BioFET structure, including the semiconductor's channel. The complete simulation allows the effects of DNA charge discretization to be reflected onto the semiconductor's channel. Furthermore, for nanoscale MOSFET, the effects of source-channel and drain-channel depletion region modulation by DNA are taken into account, thus giving a more realistic view of the total response of the device.

This paper is organized as follows: Section "Model Details" discusses the structure of the model, the mathematical equations, and the boundary conditions. Section "Results and Discussion" introduces and discusses the results of the simulations as applied to several cases of interest. Finally, section "Biosensor Design Implications" provides some design guidelines to optimize the operation of a DNA BioFET.

Model Details

The model of a BioFET consists of a FET structure, including a source diffusion, a drain diffusion, the substrate, the channel, and an insulator. Instead of a polysilicon gate, the BioFET employs an electrolyte solution and a reference electrode. The conductive electrolyte is needed to facilitate DNA immobilization and hybridization on the insulator's surface, whereas the reference electrode allows a potential to be applied to the solution that will subsequently act as a gate contact to invert the semiconductor's channel. In the finite-element model, a 2-D frontal view of the BioFET is used as shown in Fig. 1. The DNA molecules are modelled as vertical rectangles of charge extending 10 nm into the solution (around 30 bp), and with a lateral width of 2 nm, corresponding to the diameter of the DNA double helix. The DNA molecules are assumed to be impermeable to solution ions, and the charge is assumed

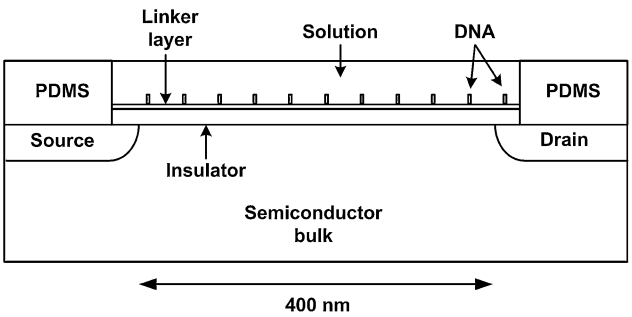

Fig. 1 2-D model of the BioFET (to scale, substrate depth truncated to save space)

to be uniformly distributed within the DNA segments. In a study by McKinnon and Landheer [18], the DNA molecule was more realistically modelled as a cylinder with a permeable charge sheet. Such a model could be incorporated here, but it would render the problem three-dimensional, with a geometric increase in the demand for computational power. As the main purpose of this paper is to study variations in the sensitivity rather than its absolute value, the 2-D model will suffice.

Aside from the geometry assumptions, there are several other assumptions to simplify the model. Firstly, the reference electrode is assumed to maintain a constant potential with respect to the solution and does not experience any drift. No possible chemical reactions of the probes or targets other than hybridization are modelled. Any effects of the buffer solution molecules, other than the salt ions, are ignored. Finally, the hybridization yield is assumed to be 100%, with complete equilibrium coverage.

The simulated transistor is of 400 nm length and 1 μm width (modelled as a multiplication factor, due to symmetry of the device in this dimension), with sufficient depth to cover the depletion width vertically. The solution is modelled as a rectangular area enclosing the DNA, with sufficient depth to cover the double-layer structure at 1-mM 1-1 electrolyte concentration. The walls of the solution wells are modelled as a PDMS layer, with a dielectric constant of 2.5. The reference electrode and the metallic contacts to the source, drain, and body connections are not modelled. The reference electrode is assumed to be a nonpolarizable electrode with a stable electrode potential. All metallic contacts are assumed to be Ohmic contacts of low resistivity, such that they can be ignored in the simulation.

Model Equations

Classical mean-field theory is used to solve the BioFET structure. This consists of Poisson's equation for potential distribution coupled with the carrier continuity equation for current flow in the semiconductor. In the absence of any gate-tunnelling current, the solution is in thermal equilibrium. The ionic concentration is then related to the electrostatic potential by the Boltzmann exponential. The mean potential profile is then given by the nonlinear Poisson–Boltzmann (PB) equation. For a z–z electrolyte, this is given by:

$$\nabla^2 V = \frac{2qn_0}{\varepsilon}\sinh(z\beta V) \tag{1}$$

In Eq. (1), V is the electrostatic potential (Volts), q is the electronic charge, ε is the permittivity of the solution medium, n_0 is the bulk salt concentration (cm^{-3}), z is the valence of the ions, and β is the inverse thermal voltage

(V^{-1}). Although the PB equation is often linearised due to small interfacial potentials, the DNA duplex is a highly charged polyelectrolyte, and it creates interface potentials higher than the thermal voltage. In addition, the interfacial potential at the insulator is a function of the applied reference electrode bias and must therefore be treated by the nonlinear PB equation.

Inside the semiconductor, the potential profile depends on the density of holes, electrons, and ionized impurities. Poisson's equation for the semiconductor's regions is therefore given by:

$$\nabla^2 V = \frac{-q}{\varepsilon}(p - n \pm N) \tag{2}$$

where p, n, and N are the volumetric densities of the holes, electrons, and ionized impurity carriers, respectively. The positive sign is taken for n-type semiconductor. In this simulation, the FET is p-type, with n-type body and p-type drain and source diffusions. The electrons and holes are not in equilibrium due to current flow. Their dependence on the potential is given by the continuity equations:

$$\begin{aligned} \nabla \cdot \vec{J}_p &= -q\nabla \cdot \left(D_p \nabla p + \mu_p p \nabla V\right) = 0 \\ \nabla \cdot \vec{J}_n &= q\nabla \cdot \left(D_n \nabla n - \mu_n n \nabla V\right) = 0 \end{aligned} \tag{3}$$

where the vectors $\vec{J}_p$ and $\vec{J}_n$ are the hole and electron current densities, respectively, D_p and D_n are the hole and electron diffusion coefficients, respectively, and μ_p and μ_n are the hole and electron mobilities, respectively. Equation (3) states that at steady state, there is no net flux of either of the carriers. The carrier current is a summation of the diffusive term and the drift term. Carrier generation and recombination currents are ignored here.

The insulator and PDMS layers are modelled using Laplace's equation:

$$\nabla^2 V = 0 \tag{4}$$

The layer for the linker molecules in this simulation are also modelled by Eq. (4), although this is only valid for a completely dense layer of linker molecules that are impermeable to ion flow. The effect of permeable linker layer on the sensitivity is given elsewhere [19]. As for the DNA molecules themselves, it is assumed that they are completely impermeable to ions and therefore are modelled by the following equation:

$$\nabla^2 V = -\frac{q n_{\mathrm{DNA}}}{\varepsilon} \tag{5}$$

where n_{DNA} is the volumetric density of DNA charges, given by $9.36 \times 10^{20}\mathrm{cm}^{-3}$ for a single-stranded DNA. This value is calculated from the geometry of the DNA molecule.

After the simulation is completed, the output current is given by the summation of electron and hole contributions to the current. For this, the following line integral must be evaluated:

$$I = W \int_{\Omega} \left(\vec{J}_p + \vec{J}_n\right) \cdot \mathrm{d}\vec{l} \tag{6}$$

where W is the width of the BioFET. In the absence of body leakage current, the boundary chosen can be the source or the drain contact or any boundary in the path of lateral current flow, such as the boundary between the source diffusion and the body.

Boundary Conditions

Two sets of boundary conditions are required to solve the problem. For the entire structure, boundary conditions for the electrostatic potential are required. In addition, boundary conditions for the carriers within the semiconductor are needed. The boundary potentials must take the corresponding material phase into consideration, since Poisson's equation solves only for the vacuum level of electrostatic potential (i.e. no chemical potential discontinuities are considered). Therefore, one must manually introduce these chemical potential differences into the boundary conditions. Failure to do so will result in the characteristics of the BioFET being shifted by the amount of the flatband potential.

For applied biases of V_g, V_b, V_s, and V_d, to the gate, body, source, and drain, respectively, the boundary conditions are given in the following equation:

$$\begin{aligned} V_{\mathrm{BG}} &= V_{\mathrm{g}} + \chi_{\mathrm{M}} - E_{\mathrm{ref}} - \chi_{\mathrm{sol}} \\ V_{\mathrm{BB}} &= V_{\mathrm{b}} + \chi_{\mathrm{M}} - \left(\chi_{\mathrm{s}} + E_{\mathrm{g}}/2 + \phi_{\mathrm{F}}\right) \\ V_{\mathrm{BS}} &= V_{\mathrm{s}} + \chi_{\mathrm{M}} - \left(\chi_{\mathrm{s}} + E_{\mathrm{g}}/2 + \phi_{\mathrm{F}}\right) \\ V_{\mathrm{BD}} &= V_{\mathrm{d}} + \chi_{\mathrm{M}} - \left(\chi_{\mathrm{s}} + E_{\mathrm{g}}/2 + \phi_{\mathrm{F}}\right) \end{aligned} \tag{7}$$

In Eq. (7), χ_{M}, χ_{s}, and χ_{sol} are the electron affinities of the metal contacts, the semiconductor, and the working ion in the solution (Cl^- in case of an Ag/AgCl reference electrode), respectively, E_{ref} is the reference electrode potential, which depends on the electrolyte concentration, E_{g} is the band gap of the semiconductor, and ϕ_{F} is the Fermi voltage of the semiconductor. It should be noted that the value of the Fermi voltage is different at the body boundary from its value at the source/drain boundaries.

As for the remaining boundaries, all external boundaries are given reflective boundary conditions, since it is assumed that there should be no potential gradients at the edges of the device. Internal boundaries are given "natural" boundary conditions requiring the continuity of the electrostatic potential as well as the continuity of the normal component of the electrostatic flux density:

$$\vec{n}_1 \cdot (\varepsilon_1 \nabla V) - \vec{n}_2 \cdot (\varepsilon_2 \nabla V) = 0 \tag{8}$$

The case of the insulator–electrolyte interface is different. Due to the chemical activity of the surface SiO groups, these sites can attract protons from the solution, causing a surface charge. This charging is the main reason behind the sensitivity of ISFET devices to the pH value of the solution. The amount of adsorbed charge σ_0 is dependent on the local pH value, which, in turn, depends on the local potential [15]. However, in this simulation, these charges were not considered. This is not to de-emphasize their adverse effects on the sensitivity of the BioFET, but rather to focus our attention on the effects of discretization and placement of DNA charges within the BioFET.

The boundary values for electrons and holes must also be specified at the edges of the semiconductor. At boundaries in contact with leads, the electron and hole densities are taken as their bulk values. This is not strictly correct, as the Ohmic potential drop within the semiconductor, due to current flow, will result in boundary values that are different from the equilibrium value. However, determining this value exactly requires a coupled solution of the BioFET with the metal–semiconductor (MS) junction. This approximation is therefore equivalent to assuming an MS junction with infinite recombination velocity (zero resistance). With this approximation in mind, the boundary conditions become:

$$\begin{aligned} n &= n_{\mathrm{i}} \mathrm{e}^{-\beta\phi_F} \\ p &= n_{\mathrm{i}} \mathrm{e}^{\beta\phi_F} \end{aligned} \tag{9}$$

where n_{i} is the intrinsic carrier density. Once again, the Fermi voltage is different at different boundaries, depending on the type and density of doping. All other external boundaries of the semiconductor structure are given reflective boundary condition, since it is not possible to overcome the potential barrier of losing carriers at these boundaries. At the boundary between the bulk and the source and drain diffusions, Neumann boundary conditions of continuous density gradients are imposed, due to the lack of any sources/sinks of carriers.

Solution

The simulation was carried out using a commercial solver (COMSOL multiphysics). The finite element mesh was automatically generated for the structure, but with controlled distribution and increased density in the regions close to the insulator. However, due to the severe nonlinearities in the model, as well as the varying characteristic length scales, coupled multiphysics simulations are not easily solved. It becomes necessary to provide close initial estimates of the solution before the perturbed solution can be calculated.

Another problem with the coupled simulation is that the ranges of the three solved variables (V, n and p) are very different, and their variations differ significantly within the BioFET. The potential V varies only in the range of ~ 1 V, with quadratic to exponential profiles, whereas the electron and hole densities vary in the range of $\sim 10^{17}\mathrm{cm}^{-3}$, with variation profiles that are super-exponential. Such a huge difference in the variables makes it hard to choose an efficient mesh and results in much longer simulation times and larger errors.

To circumvent the first convergence problem, a good initial guess for the potential and charge must be carried out. One way to do this is to solve a similar problem in complete thermal equilibrium (i.e. body, drain, and source all at the same potential). In this case, Eq. (1) does not change, but Eq. (2) is no longer a coupled equation and can be written in terms of the potential alone as follows:

$$\begin{aligned} \nabla^2 V = \frac{-q}{\varepsilon}\Big(& n_{\mathrm{i}} \mathrm{e}^{-\beta\left(V-\left(V_{\mathrm{b}}+\chi_{\mathrm{M}}-\left(\chi_{\mathrm{s}}+E_{\mathrm{g}}/2\right)\right)-\phi_{\mathrm{F}}\right)} \\ & - n_{\mathrm{i}} \mathrm{e}^{\beta\left(V-\left(V_{\mathrm{b}}+\chi_{\mathrm{M}}-\left(\chi_{\mathrm{s}}+E_{\mathrm{g}}/2\right)\right)-\phi_{\mathrm{F}}\right)} \pm N\Big) \end{aligned} \tag{10}$$

Therefore, in the thermal equilibrium case, a single nonlinear problem in the potential alone can be solved. The obtained solution can then be used as an initial guess in the solution of the perturbed case. However, this may still not be enough, and one might have to "soft start" the transistor starting from very low drain biases and with small increments, using the result of each simulation as an initial guess to the subsequent simulation.

The problem of variation in the variables' ranges can be solved by using a substitution. In particular, the "quasi-Fermi" formulation can be used with the following substitutions:

$$\begin{aligned} p &= n_{\mathrm{i}} \mathrm{e}^{-\beta\left(V-V_{\mathrm{qfp}}+\chi_{\mathrm{Si}}+E_{\mathrm{g}}/2\right)} \\ n &= n_{\mathrm{i}} \mathrm{e}^{\beta\left(V-V_{\mathrm{qfn}}+\chi_{\mathrm{Si}}+E_{\mathrm{g}}/2\right)} \end{aligned} \tag{11}$$

where the new variables are the quasi-Fermi potential for holes V_{qfp} and electrons V_{qfn}. These new variables vary in the same range as V, and the simulation is therefore faster and more accurate. The simulation parameters are given in Table 1.

Table 1 Simulation parameters

Parameter	Value	Unit
Ion concentration	1	mM
Substrate doping	3×10^{16}	cm^{-3}
Diffusion doping	10^{19}	cm^{-3}
Temperature	300	K
Device length	400	nm
Device width	1,000	nm
Base pairs	30	–
DNA spacings	20	nm
Insulator thickness	18	nm

Results and Discussion

Current–voltage plots were obtained from 1-D [15] and 2-D simulations for comparison. Figure 2 shows the results for three different gate-source voltages. The threshold voltage of this BioFET is determined to be −1.3 V. The absence of the channel-length modulation effect in saturation is clear from these plots as the charge-sheet model used in 1-D simulations does not capture this effect, i.e. a long-channel model was used since the channel-length modulation factor is semi-empirical in its derivation. Additionally, the 2-D model predicts a higher current in deep inversion because the current is calculated along the entire depth profile of the channel (sub-surface conduction) and not based on a charge sheet as in the 1-D model.

The BioFET signal is defined as the difference in the drain current between a surface with hybridization and a surface without hybridization. In the model, this is calculated by performing two simulations, one with double the DNA density of the other and calculating the difference in the observed current. Figure 3a shows simulation results of the BioFET current at different drain and gate biases. The 1-D simulation is seen to overestimate the observed signal, particularly at deep inversion. The reduction in sensitivity is explained by the lateral ionic shielding of the DNA molecule, which prevents the electric fields from causing additional inversion in the channel of the semiconductor. Such an effect cannot be quantified using a simple 1-D model for the BioFET. Furthermore, the ratio between the 2-D and 1-D simulations, shown in Fig. 3b, gives a minimum value close to 40%, illustrating that the 1-D simulation can result in an error of around 60%. For deep inversion, these results agree with those of McKinnon and Landheer [18], where it was stated that variations in the range of 50% are expected for the simulated range of electrolytic concentration and DNA density. However, the weak inversion result here shows that the 2-D model approaches the results of the 1-D model, emphasizing the importance of the 1-D model in determining the device's sensitivity in low inversion. In any case, these results illustrate that the geometry of the biomolecule is an important factor and must be considered in modelling attempts. This is particularly important at high electrolyte concentrations and in deep inversion.

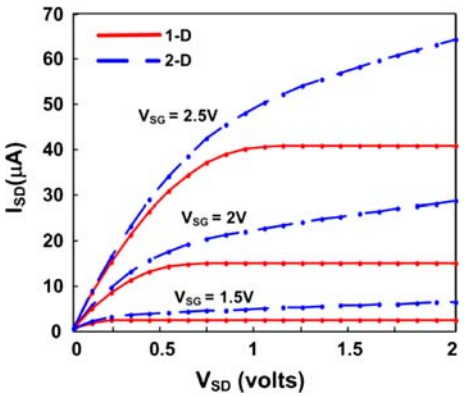

Fig. 2 Drain current versus voltage BioFET simulations

The finite-element model has also been used to investigate the effect of the position of the probes along the channel of a nanoscale sensor. Figure 4 shows simulation results of the BioFET signal for different sample distributions of the probe molecules. Four such simulation sets were conducted, with the probes distributed (1) uniformly, (2) aggregated around the centre, (3) aggregated closer to the source terminal, and (4) aggregated closer to the drain terminal. The simulation shows that the uniform, sparsely spaced DNA probes give the highest sensitivity. This might sound intuitive as the conductivity of the BioFET channel would increase optimally when the charge increase is distributed along the direction of current flow (conductances in series). However, as the DNA probes are placed farther apart, the shielding ability of the ionic cloud increases, and one would expect that the effective amount of conductance change in the channel will be reduced. This is in contrast to the case with aggregated DNA probes, where the ionic cloud is not as efficient in shielding the charge of the DNA, and more localized inversion is thus expected. The

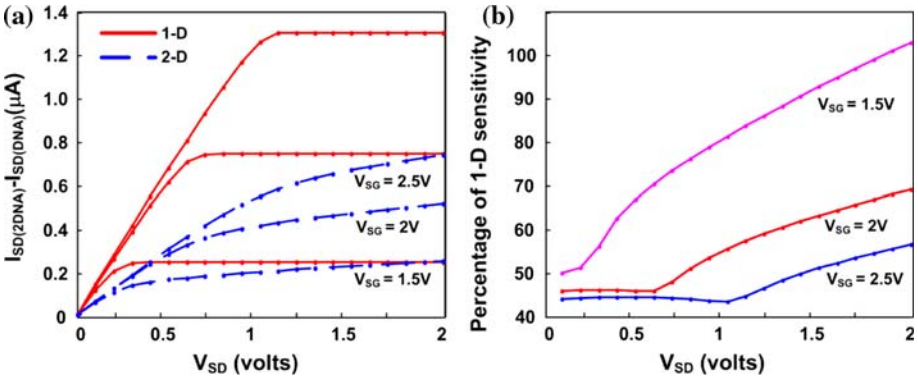

Fig. 3 **a** Simulation results of BioFET hybridization currents in 1-D and 2-D, **b** ratio between 2-D and 1-D results

simulation, however, shows that even for a short-channel BioFET, uniform distribution of inversion charges is more important.

When the probes are placed closer to the centre, source, or drain, the sensitivity of the device is significantly reduced. The source and drain ends seem to be less sensitive to the DNA charge than the centre. This can also be explained by noting that the drain and source surface potentials are much harder to modulate by charges on the gate, as they are in electrical contact with the drain and reservoirs. The harder charge modulation makes it more difficult for the DNA targets to induce an electrical signal. In the case of the drain aggregated probes, another phenomenon is noticed. As the device is put in deep saturation, the BioFET is desensitized. The channel pinch-off in saturation is responsible for this. On the onset of saturation, the drain's ability to draw charges is dramatically increased, and the lateral electric field becomes very strong. The weak modulation of the vertical electric field due to hybridization will not result in any significant change in the underlying local surface potential, and the BioFET is desensitized along this region. In this case, several probes that are in close proximity to the drain are made redundant and will only weakly contribute to the total current change.

From Fig. 4, one can see that for any drain bias, placement of the probe DNA can change the sensitivity of the device by around 50%. The BioFET is, therefore, extremely sensitive to variations in DNA immobilization profile, which in itself depends on the lateral profile of the linker molecules. This is directly attributed to the asymmetric distribution of charges within the channel of the FET and places a limit on nanobiosensor design, where the channel is dominated by short-channel effects. For long-channel devices, the diffusion-controlled regions extend minimally over the channel, with the largest region of the channel being drift-controlled (resistive). The variance in probe placements will, therefore, not have detrimental effects on the operation of the BioFET, unless the DNA aggregation is severe. However, assuming purely entropic diffusion of probes during immobilization, such an aggregation is not likely to occur.

A final observation using the 2-D model is regarding nonspecific charges. The sensitivity of the device to hybridization charges is quite different than to immobilization charges. This effect can be quantified only with complete geometric modelling of the immobilized probe molecules. In general, many different phenomena can contribute to signals that obscure the sensor's signal. Examples include target adsorption by the linker molecules, spurious protein bindings, and ionic adsorption. The hybridization charge is localized at the same locations of the probes, whereas spurious adsorption can occur anywhere on the surface. Intuitively, one would expect that the spurious adsorptions might induce a smaller signal, because they increase the screening area for the charges and can thus be screened more efficiently (as opposed to sharing the ionic screening area with the capturing probe). However, the nonlinearity of the double-layer screening, as well as the more distributed inversion charge on the semiconductor due to the occupancy of vacant surface positions by the adsorbents, cause the corresponding BioFET's signal to be higher by several times than the signal due to legitimate, specific target capture. Figure 5 shows simulation results of the BioFET's current for complementary hybridization, as well as for spurious adsorption of molecules of similar structure carrying the same charge (modelled here by doubling the probe molecules' density and distributing them evenly). The simulation shows more than fivefold increase in the sensed current due to erroneous charges. These erroneous bindings are often noncovalent and can therefore be rinsed away prior to making the measurements. However, the rinsing and replenishing processes can cause changes in the ionic characteristics of the solution; that might lead to more signal discrepancy. This also limits the potential use of this biosensor to monitor the kinetics and dynamics of the DNA surface hybridization.

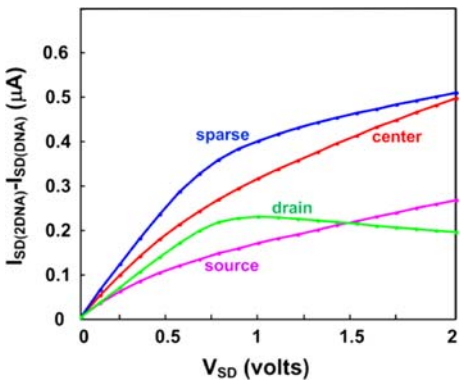

Fig. 4 Simulation results of the BioFET current for difference DNA aggregates

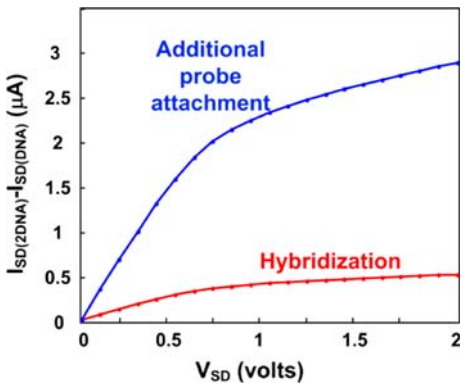

Fig. 5 Drain current versus voltage BioFET simulations

Biosensor Design Implications

The preceding simulations can be used to monitor and quantify several effects and assess their significance to the design of the BioFET. These effects are to be considered as sources of random variations between the cells of fully electronic DNA microarrays. As mentioned previously, such effects are more pronounced in nanoscale sensors, such as sub-micron FETs. To minimize erroneous readings and variations, several measures must be taken at the chemical synthesis level, as well as at the circuit level.

At the chemical level, the environmental conditions during the linker-building process, as well as the probe attachment process, must be carefully selected to ensure mean equilibrium spacings that are small in comparison with the device geometry. This will desensitize the sensor to the Brownian variance in positioning of the linkers and probes. However, care must be taken as a very dense DNA layer can severely hinder hybridization due to the steric barriers involved. Additionally, a very dense linker layer will transform the layer into the "brush" regime [20], possibly with serious conformation and DNA immobilization consequences. Thus, the exposure time for immobilization must be long enough such that statistical biases are not amplified but must not be too long to render the layer impermeable to targets. The unused linker molecules should be deactivated so that they only act as ionic barriers but not as energy wells for adsorption.

At the circuit level, differential configurations should be used to eliminate all common sources of variations, such as reference electrode drift, solution's pH or ionic strength variations, temperature, or nonspecific binding. The roles of the positive and negative BioFETs should be interchanged (via a chopper circuit, for example), to eliminate other common-mode biases due to fabrication or surface chemistry variations. Finally, the symmetry of the MOSFET should be utilized in interchanging the roles of the source and drain terminals and averaging the readings out. This will minimize reading errors due to positioning variations of the probes. Drain potential sweeps can be carried out and compared to the model to study the distribution of the probes.

Conclusion

The unique capability of nanoscale sensors to detect biological and chemical substances is complicated by their extreme sensitivity to the sizes, placements, and energetics of the active species, as well as those of cross-reactions. Studying the effects of these factors requires deep physical modelling of these sensors. Mean-field finite-element modelling has been used to quantify the signal variations due to several common phenomena in biosensors. It is shown that poor level of control during fabrication is very likely to result in significant errors in signal reading. This model can also be integrated with molecular dynamics models or Monte Carlo simulations to assist in the study of noise in biosensors. Proper physical simulation will allow the identification of fabrication targets that allow commercial, low-cost fabrication of such sensors with high accuracy and reliability.

Acknowledgments The authors would like to acknowledge support from the Canada Research Chair program, the Natural Sciences and Engineering Research Council (NSERC) of Canada. In addition, the final version of this manuscript was prepared while Dr. M.J. Deen was a WCU Distinguished Visiting Professor and Waleed Shinwari was a Visiting Scholar at POSTECH, Pohang, South Korea, under the auspices of the Ministry of Education, Science, and Technology Program—Project no. R31-2008-000-10100-0—and their support is gratefully acknowledged.

References

1. W. Cai, J.R. Peck, D.W. van der Weide, R.J. Hamers, Biosen. Bioelec. **19**, 1013 (2004)
2. K.M. Millan, A. Saraullo, S.R. Mikkelsen, Anal. Chem. **66**, 2943 (1994)
3. T.G. Drummond, M.G. Hill, J.K. Barton, Nat. Biotechnol. **21**, 1192 (2003)
4. E. Souteyrand et al., J. Phys. Chem. B **101**, 2980 (1997)
5. F. Uslu, S. Ingebrandt, D. Mayer, S. Böcker-Meffert, M. Odenthal, A. Offenhäusser, Biosen. Bioelec. **19**, 1723 (2004)
6. T. Sakata, M. Kamahori, Y. Miyahara, Jpn. J. Appl. Phys. **44**, 2854 (2005)
7. M.W. Shinwari, M.J. Deen, D. Landheer, Microelectron. Reliab. **47**, 2025 (2006)
8. R. Mukhopadhyay, M. Lorentzen, J. Kjems, F. Besenbacher, Langmuir **21**, 8400 (2005)
9. M. Su, S. Li, V.P. Dravid, Appl. Phys. Lett. **82**, 3562 (2003)
10. G. Di Francia, V. La Ferrara, S. Manzo, S. Chaivarini, S. Chaivarini, Biosen. Bioelec. **21**, 661 (2004)
11. J. Hahm, C. Lieber, Nano Lett. **4**, 51 (2004)
12. J. Reichert, A. Csáki, J.M. Köhler, W. Fritzsche, Anal. Chem. **72**, 6025 (2000)
13. J. Nam, S.I. Stoeva, C.A. Mirkin, J. Am. Chem. Soc. **126**, 5932 (2004)
14. M.J. Deen, M.W. Shinwari, J.C. Ranuárez, D. Landheer, J. Appl. Phys. **100**, 074703 (2006)
15. D. Landheer, G. Aers, W.R. McKinnon, M.J. Deen, J.C. Ranuárez, J. Appl. Phys. **98**, 044701 (2005)
16. D. Landheer, W.R. McKinnon, G. Aers, W. Jiang, M.J. Deen, M.W. Shinwari, IEEE Sens. J. **7**, 1233 (2007)
17. M.W. Shinwari, M.J. Deen, P. Selvaganapathy, IET Circ. Dev. Sys. **2**, 158 (2008)
18. W.R. McKinnon, D. Landheer, J. Appl. Phys. **100**, 054703 (2006)
19. M.W. Shinwari, M.J. Deen, *1st MNRC2008*, vol. 185 (2008)
20. A. Halerpin, A. Buhot, E.B. Zhulina, Biophys. J. **89**, 796 (2005)